Journal of Hydrology 456–457 (2012) 130–138

Contents lists available at SciVerse ScienceDirect

Journal of Hydrology

journal homepage: www.elsevier.com/locate/jhydrol

Summertime evaluation of REFAME over the Unites States for near real-time high resolution precipitation estimation

Ali Behrangi [a,*], Soroosh Sorooshian [b], Kuo-lin Hsu [b]

[a] Jet Propulsion Laboratory, California Institute of Technology, Pasadena, CA, USA
[b] Center for Hydrometeorology and Remote Sensing (CHRS), The Henry Samueli School of Engineering, Dept. of Civil & Environmental Engineering, University of California, Irvine, CA, USA

ARTICLE INFO

Article history:
Received 9 March 2012
Received in revised form 4 June 2012
Accepted 10 June 2012
Available online 26 June 2012
This manuscript was handled by Konstantine P. Georgakakos, Editor-in-Chief, with the assistance of Emmanouil N. Anagnostou, Associate Editor

Keywords:
Precipitation
Remote sensing
Microwave
Hydrology
Real-time
Global
REFAME

SUMMARY

Precipitation is the key input for hydrometeorological modeling and applications. In many regions of the world, including populated areas, ground-based measurement of precipitation (whether from radar or rain gauge) is either sparse in time and space or nonexistent. Therefore, high-resolution satellite-based precipitation products are recognized as critical data sources, especially for rapidly-evolving hydrometeorological events such as flash floods which primarily occur during summer/warm seasons. As "proof of concept", a recently proposed algorithm called Rain Estimation using Forward Adjusted-advection of Microwave Estimates (REFAME) and its variation REFAMEgeo are evaluated over the contiguous United States during summers of 2009 and 2011. Both methods are originally designed for near real-time high resolution precipitation estimation from remotely sensed data. High-resolution Q2 (ground radar) precipitation data, in conjunction with two operational near real-time satellite-based precipitation products (PERSIANN, PERSIANN-CCS) are used as evaluation reference and for comparison. The study is performed at half-hour temporal resolution and at a range of spatial resolutions (0.08-, 0.25-, 0.5-, and 1-degree latitude/longitude). The statistical analyses suggest that REFAMEgeo performs favorably among the studied products in terms of capturing both spatial coverage and intensity of precipitation at near real-time with the temporal resolution offered by geostationary satellites. With respect to volume precipitation, REFAMEgeo together with REFAME demonstrates slight overestimation of intense precipitation and underestimation of light precipitation events. Compared to REFAME, It is observed that REFAMEgeo maintains stable performance, even when the amount of accessible microwave (MW) overpasses is limited. Based on the encouraging outcome of this study which was intended as "proof of concept", further testing for other seasons and data-rich regions is the next logical step. Upon confirmation of the relative reliability of the algorithm, it is reasonable to recommend the use of its precipitation estimates for data-sparse regions of the world.

1. Introduction

Near real-time high-resolution precipitation data are critical to a wide range of hydrometeorological studies and applications. The report by National Weather Service (http://www.weather.gov/floodsafety/floodsafe.shtml) indicates that flooding is the 1st ranked source of damage in the US compared to the other weather-related events during the last 30 years. According to a report by the World Water Assessment Programme (2009), more than 7000 major disasters (flood/drought) have been recorded worldwide since 1970, causing at least $2 trillion in damage and killing at least 2.5 million people. A key input into flood forecasting models is near real-time precipitation data. While only a few countries are equipped with a dense network of ground-radar and gauge measurements, in many regions of the world near real-time high-resolution precipitation data can only be obtained from remotely sensed estimates. Besides the Tropical Rainfall Measuring Mission (TRMM) precipitation radar, currently, passive microwave (MW) sensors provide the most reliable instantaneous precipitation estimates at global scale. These sensors are aboard Low Earth orbiting (LEO) satellites, restricting the temporal resolution of precipitation monitoring. On the other hand, Geosynchronous Earth-orbiting (GEO) satellites provide high-resolution visible (VIS) and infrared (IR) images (typically at 0.04-degree latitude/longitude grid boxes every half-hour or less) which are useful for high-resolution monitoring of precipitation systems. However, precipitation estimation from IR imagery relies on cloud-top information, and it is generally less accurate than MW-based precipitation retrievals.

* Corresponding author. Address: Jet Propulsion Laboratory, California Institute of Technology, 4800 Oak Grove Drive, MS 233-304, Pasadena, CA 91109, USA. Tel.: +1 818 3938657.
E-mail addresses: ali.behrangi@jpl.nasa.gov (A. Behrangi), soroosh@uci.edu (S. Sorooshian), kuolinh@uci.edu (K. Hsu).

0022-1694/$ - see front matter © 2012 Elsevier B.V. All rights reserved.
http://dx.doi.org/10.1016/j.jhydrol.2012.06.033

Recognition of the above-described benefits and limitations has motivated the development of several precipitation retrieval algorithms to combine information from MW and IR sensors aboard LEO and GEO platforms (Huffman et al., 2007; Joyce et al., 2004; Kidd et al., 2003; Kuligowski, 2002; Sorooshian et al., 2000; Turk et al., 2000; Ushio et al., 2009, among others). For near real-time precipitation estimation, the role of rapidly updated IR images from GEO-satellites is critical. Therefore, three general strategies have been employed. The first and the most common type of strategy is retrieving precipitation intensity directly from GEO images by establishing an empirical relationship between IR brightness temperature (Tb) and the corresponding microwave precipitation estimates. The main difference among such retrieval methods is based on the technique used to establish the Tb–precipitation rate (PR) relationship and may include histogram matching (e.g., Kidd et al., 2003; Turk et al., 2000), regression (e.g., Kuligowski, 2002), or neural network (e.g., Hsu et al., 1997; Sorooshian et al., 2000) techniques. In all of the methods used to establish the Tb–PR relationship, the more intense precipitation will be generally assigned to clouds with lower Tb at the top. This might be a valid assumption for convective clouds. However, the inverse relationship is not always true. High-altitude cirrus clouds, for instance, are very cold and mistakenly depicted as raining by IR-only algorithms. Conversely, lower-level clouds that produce rain are assigned as non-raining clouds to IR-only algorithms. While multi-spectral information from GEO visible (VIS) and water vapor (WV) bands has been found effective to improve precipitation detection and estimation from GEO platforms (e.g., Ba and Gruber, 2001; Behrangi et al., 2009, 2010), the lack of interaction with hydrometeors is still a major drawback of the GEO-based precipitation estimation techniques.

In the second type of the combined algorithms, applicable for near real-time precipitation estimation, precipitation rate is derived exclusively from MW sensors. In other words, through forward-only propagation of precipitation along IR-derived cloud motion vectors, a temporally and spatially complete precipitation field can be obtained (see forward-only calculations in Joyce et al., 2004). With this approach, MW precipitation intensity captured by the previous MW overpass is only advected and remains unchanged until the next MW overpass becomes available. Arguably, this may cause an overestimation of precipitation if the previous pass from a MW-sensor scans a mature convective precipitation system that is about to start its decaying phase. Conversely, if the previous MW-sensor collects samples from the initial stage of a growing convective precipitation system, the forward-only advection method may yield a considerable underestimation of both precipitation intensity and areal extent. Recognizing the issue, the Global Satellite Mapping of Precipitation (GSMaP) project has employed a Kalman filtering approach to adjust the propagated precipitation intensities using frequent observation of cloud top Tb to produce a high-resolution near real-time precipitation product (GSMaP-NRT, Ushio et al., 2009). It is important to note that both groups provide forward–backward interpolated products (CMORPH, GSMaP-MVK), which are basically weighted averaging of advected MW precipitation from the previous and subsequent MW overpasses. The reliance of CMORPH and GSMaP-MVK to the next MW overpass improves the performance of the products compared to their corresponding forward-only products. However, the next MW overpass may not appear until several hours, which may hamper the near real-time monitoring of precipitation events.

The third combination strategy for near real-time applications is based on obtaining the "best" local estimate for a given grid box. The 3B42-RT product of the TRMM Multi-satellite Precipitation Analysis (TMPA; Huffman et al., 2007) relies on collecting available MW precipitation estimates from various satellites within a fixed time bracket of 3 h and then filling the remaining gaps with MW-calibrated IR estimates. The 3-h time bracket is the best temporal resolution offered by 3b42-RT and is a trade-off between collection of enough MW overpasses and precipitation production at near real-time.

In continuation of the described efforts, Behrangi et al. (2010) suggested an algorithm called Rain Estimation using Forward Adjusted-advection of Microwave Estimates (REFAME) that incorporates a GEO-based multi-feature cloud-classification technique to adjust MW precipitation intensities as advected along cloud-motion streamlines. The proposed algorithm is flexible because it uses a wide array of precipitation-relevant information to improve the cloud- classification component and, as a result, the adjustment of precipitation intensities in near real-time. Behrangi et al. (2010) also suggested a variation of REFAME called REFAMEgeo, which combines precipitation intensities calculated from REFAME and GEO/IR.

The present manuscript evaluates the performance of REFAME and REFAMEgeo over the contiguous United States using high-resolution ground-radar precipitation data and two operational satellite-based products that offer near real-time precipitation estimation with spatiotemporal resolutions comparable to REFAME and REFAMEgeo. The study is focused on summertime over the United States because:

(a) The original goal of the proposed algorithms is for hydrologic applications that require near real-time high resolution estimation of rainfall (i.e. useful for monitoring rapidly evolving floods). The important role of high resolution precipitation data for flood-related hydrologic simulations is highlighted in Nikolopoulos et al. (2010). Naturally, our evaluation strategy should be towards our original goal. Majority of flash floods (rapidly evolving floods) occur during summertime. Therefore, by focusing on summer the algorithms can be evaluated under conditions that high resolution precipitation estimation data are needed the most.
(b) United States has a significantly dense network of ground precipitation measurements over a large region covering different weather and climate regimes. Therefore, similar to several other studies and at least as a first step, it is reasonable to take advantage of such dense measurements to verify the performance of satellite-based precipitation products and also for proof of concept for newly developed algorithms, and
(c) Within the resolution of our study (30 min, 0.08°) more than 1 billion pairs of satellite-radar precipitation data were collected which creates a valuable dataset for our evaluation and comparison purposes at high resolution.

Another hope and expectation from this "proof of Concept" study is that if the testing of the proposed algorithms over a data-rich area (e.g., over the US) exhibits reasonable skills, then it can be applied quasi-globally to provide critical high resolution precipitation data especially over regions with sparse or nonexistent ground measurements. Clearly, quality verification of high resolution precipitation products over other regions remains to be an important but a difficult task due to availability and reliability issues associated with ground measurements of precipitation.

A brief overview of REFAME and REFAMEgeo is provided in Section 2. In Section 3, area and period of study as well as input data sets used in this study are described. Description of reference precipitation dataset including ground radar and satellite precipitation products is also provided in Section 3. The evaluation results are reported and discussed in Section 4, and summary and concluding remarks are presented in Section 5.

2. An overview of REFAME and REFAMEgeo

While a more complete description of REFAME can be obtained from Behrangi et al. (2010), a brief overview of the algorithm is provided in this section. Within a Lagrangian framework, REFAME provides a spatially complete MW adjusted-precipitation field at 0.08-degree resolution every half-hour and includes the following three steps: First, a recently developed 2-D cloud-tracking algorithm (Bellerby, 2006; Bellerby et al., 2009) is employed to derive cloud-motion vectors from successive high- resolution (0.04-degree latitude/longitude every 30 min) IR images. The tracking algorithm is computationally efficient and has been shown to be effective in the presence of image rotation and shear and accurate to within 2–3 pixels (Bellerby, 2006). The tracking algorithm allows REFAME to explicitly incorporate the effect of cloud motion, growth, deformation, and dispersal (decay). In the second step, radiative (Tb), textural (e.g., standard deviation of Tbs of neighboring grid boxes), and dynamic (gradients of Tb between successive IR images) features of clouds are extracted and employed to classify cloudy scenes into 400 distinct clusters. Using ground precipitation data, a mean precipitation rate (MPR) is calculated for each cluster. The third step includes the adjustment of advected MW precipitation rates along cloud-motion streamlines. For each individual grid box at time t, an adjustment-coefficient is identified by dividing the MPR of the corresponding cluster at time t by the MPR of the corresponding cluster at time t-1 along the cloud-motion streamlines. After multiplying the advected MW precipitation rate by the calculated adjustment-coefficient, the adjusted-advection of the MW precipitation estimate for each grid box is obtained.

As described in Behrangi et al. (2010), the addition of the intensity-adjustment procedure proposed in REFAME is effective and results in improved statistical scores compared to a scenario that relies only on advection of MW precipitation rates. However, with the reported setup, REFAME cannot account for precipitation events that are not observed in previous MW overpasses because the adjustment procedure is multiplicative. Among such events, convective precipitation systems that are often responsible for flash floods are critical because they may grow from initiation to a mature stage within a few hours or less. If the most recent MW overpass happens prior to the initiation phase of the system, the precipitation rate can only be captured by GEO-based precipitation retrieval methods. Recognizing this issue, REFAMEgeo was proposed (Behrangi et al., 2010). By assigning proper weights to each precipitation estimate, REFAMEgeo combines precipitation intensities calculated from REFAME and GEO/IR data. The combination weights are obtained by analyzing the overall performance of the two precipitation estimates with respect to a reference precipitation measurement and for each time distance from previous MW overpasses. In order to derive precipitation rates from GEO/IR information, a method described in Behrangi et al. (2009) incorporated a cloud-classification scheme to establish a Tb-rain rate relationship. In Section 4, both near real-time precipitation products (REFAME and REFAMEgeo) are evaluated and cross-compared with their counterparts.

3. Study area and data set

The evaluation study is performed over the contiguous United States during the summer (June, July, and August) of 2009 and 2011 using half-hour ground radar precipitation dataset. During summer rapidly-evolving precipitation systems are more frequent than other seasons which allow evaluation of REFAME and REFAMEgeo over a period of time when maintaining high temporal resolution is critical. In addition, quality of radar ground measurements during winter, when snow and near surface mixed phase precipitation occurs, is less reliable for evaluation of precipitation products.

The datasets used in the present study are described below. All of the datasets were remapped to common 30-min 0.08-degree latitude/longitude resolution grid maps in the present study.

3.1. Data set used to generate REFAME and REFAMEgeo

The inputs to REFAME and REFAMEgeo include GEO-IR images and precipitation intensities from MW sensors. Half-hourly $0.04^\circ \times 0.04^\circ$ GEO-IR data were obtained from the National Oceanic and Atmospheric Administration/National Environmental Satellite, Data, and Information Service (NOAA/NESDIS) Environmental Satellite Processing Center (ESPC) over the conterminous United States. MW precipitation intensities are obtained from the CPC MW combined precipitation product (hereafter referred to as MWCOMB). For the period and location of the present study, MWCOMB includes: (1) the Advanced Microwave Sounding Unit-B (AMSU-B) sensors on NOAA polar-orbiting operational meteorological satellites (NOAA 15, 16, 17); (2) the Microwave Humidity Sounder (MHS) on NOAA 18, 19, and MetOp; (3) the Special Sensor Microwave Imager (SSM/I) on the US Defense Meteorological Satellite Program (DMSP) satellite F-13; (4) the Tropical Rainfall Measuring Mission (TRMM) Microwave Imager (TMI); and (5) the Advanced Microwave Scanning Radiometer (AMSR-E) on Aqua. The latest Goddard profiling (GPROF) rainfall-estimation algorithm (Wilheit et al., 2003) is used to generate precipitation from TMI, AMSR-E, and SSM/I brightness temperature channels. For MHS and AMSU-B, the NESDIS AMSU-B rainfall algorithm (Ferraro, 1997; Vila et al., 2007) is employed to derive precipitation rates. MWCOMB contains half-hour inter-calibrated MW precipitation estimates at 0.0727-degree latitude/longitude resolution, in addition to flags for MW sensor type. More detailed descriptions of the computational procedure and specifications of the MWCOMB can be obtained from Joyce et al. (2004).

3.2. Reference ground precipitation data set

The National Mosaic and Quantitative Precipitation Estimation (QPE) system (NMQ/Q2) (Vasiloff et al., 2007; Zhang et al., 2009; http://www.nmq.ou.edu) was used as reference precipitation. Q2 has been developed at the NOAA/National Severe Storms Laboratory in cooperation with the University of Oklahoma and employs data-quality control, multi-sensor precipitation classification, multi-sensor QPE, and evaluation components to create high spatial and temporal resolution precipitation estimates for flood warnings and water-resources management on the national scale. The Q2 system generates QPE products at 1-km horizontal resolution with a 5-min update cycle. For consistency among different datasets, in the present study, the Q2 data were remapped to common 30-min 0.08-degree latitude/longitude resolution.

3.3. High-resolution satellite-based precipitation products

In Section 2, different approaches were described to derive a temporally and spatially complete field of high-resolution precipitation intensities. The first approach derives precipitation intensities from GEO-IR images, and MW precipitation estimates are essentially used to establish and update the Tb-rain rate relationships. The second approach derives precipitation intensities directly from MW precipitation estimates, and GEO-IR images are used mainly to propagate the MW estimates in time and space. Therefore, for both approaches the role of GEO images is critical to produce near real-time precipitation estimation. In the present study, two products are selected for cross-comparison with REFAME and REFAMEgeo. These two products are Precipitation

Estimation from Remotely Sensed Information using Artificial Neural Networks (PERSIANN; Sorooshian et al., 2000; Hsu et al., 1997) and the PERSIANN cloud-classification system (PERSIANN-CCS; Hong et al., 2004). Both products provide half-hour precipitation estimation identical to the time resolution offered by REFAME and REFAMEgeo. PERSIANN-CCS is a patch-based approach that is available quasi-globally (60°S to 60°N) every half-hour at 0.04-degree latitude/longitude resolution. PERSIANN, on the other hand, is a pixel-based approach that derives precipitation rates at a quasi-global (60°S to 60°N) scale every half-hour and at 0.25-degree resolution. Both PERSIANN and PERSIANN-CCS derive precipitation rate directly from GEO infrared images based on establishing relationships between infrared brightness temperature and rain rate using training datasets. While PERSIANN-CCS has been operational since 2006, employed relationships between brightness temperature and rain rate are based on initial trainings using one-year of global MW rain rates.

4. Results

Fig. 1 shows a density scatter plot of half-hour REFAME (Fig. 1a), REFAMEgeo (Fig. 1b), PERSIANN-CCS (Fig. 1c), and PERSIANN (Fig. 1d) precipitation estimates (*y*-axis) versus the reference half-hour Q2 precipitation rates (*x*-axis) at 0.5-degree resolution. For precipitation rates between 0.1 mm/hr and 64 mm/hr, both axes are divided into 100 evenly divided spaces in the logarithmic scale, and the number of samples inside each grid box is counted. The favorable case is to have the highest concentration of the precipitation intensities symmetrically distributed along the 1:1 line shown in each panel. Therefore, although both REFAME (Fig. 1a) and REFAMEgeo (Fig. 1b) demonstrate a relatively high concentration of samples along 1:1 line, REFAMEgeo is considered the best.

Fig. 2 displays fractions of precipitation volume (*y*-axis) versus precipitation intensity (*x*-axis) derived from half-hour 0.25-degree REFAME, REFAMEgeo, PERSIANN, and PERSIANN-CCS products. Only precipitation rates between 0.1 mm/hr and 64 mm/hr are included in Fig. 2 and the volume fractions are calculated for 100 evenly divided precipitation-intensity bins in the logarithmic scale. Q2 is considered as reference; therefore, the area below the Q2 curve is equal to one unit. For precipitation rates less than approximately 4 mm/hr, the products, especially PERSIANN-CCS, demonstrate considerable underestimation of precipitation volume. However, at higher rain intensity ranges the products overestimate the volume of total precipitation. Among the products, PERSIANN shows a larger overestimation of rain intensities between 3 mm/hr and 20 mm/hr and PERSIANN-CCS only displays overestimations for rain rates between 5 mm/hr and 16 mm/hr. The rain volume distributions of REFAME and REFAMEgeo are similar to that of PERSIANN at rain intensities less than about 3 mm/hr. However, at higher intensities REFAME and REFAMEgeo show less overestimations compared to PERSIANN. Note that the rain volume distribution of REFAME and REFAMEgeo are fairly similar across the range of rain intensities. It is worth mentioning that the relatively different rain volume distribution of PERSIANN-CCS could be related to two issues: (a) PERSIANN-CCS is not updated in near-real-time using MW precipitation dataset. Therefore, unlike REFAME, REFMEgeo and PERSIANN, it is independent of newly available MW precipitation data; (b) unlike PERSIANN and REFAMEgeo, PERSIANN-CCS follows a patch-based concept where Tb-rain rate relationship is established for each class of cloud after performing cloud segmentation and classification processes.

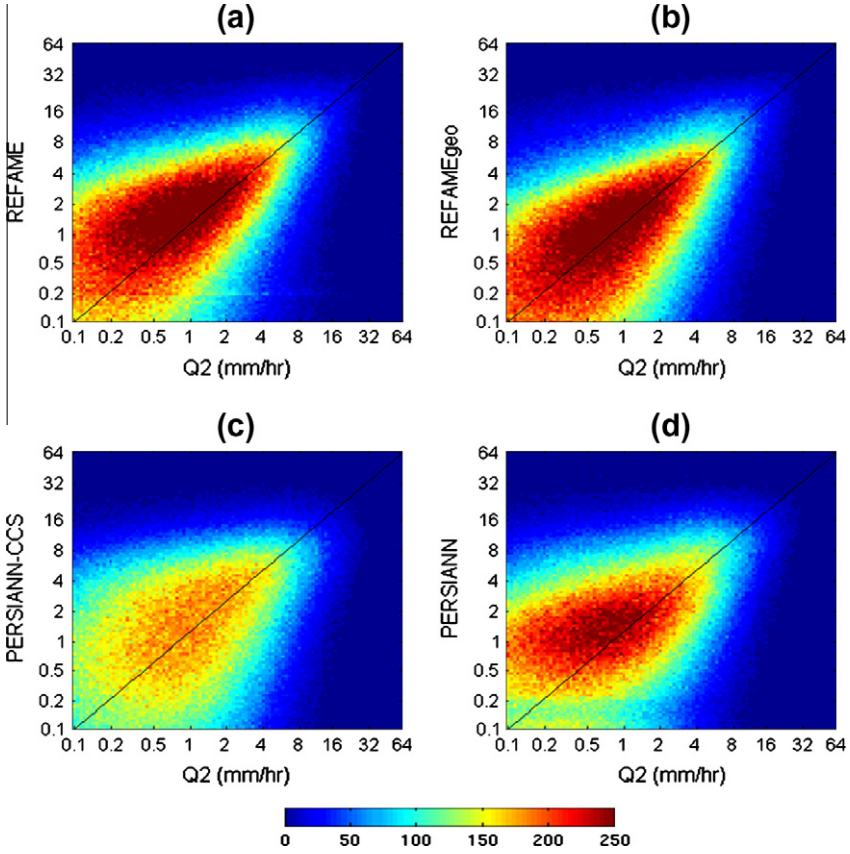

Fig. 1. Density scatterplot of half-hour REFAME (panel a), REFAMEgeo (panel b), PERSIANN-CCS (panel c), and PERSIANN (panel d) precipitation estimates (*y*-axis) versus the reference half-hour Q2 precipitation rates (*x*-axis) at 0.5-degree resolution. Both axes are divided into 100 evenly divided spaces in logarithmic scale, and the number of samples inside each grid box is counted.

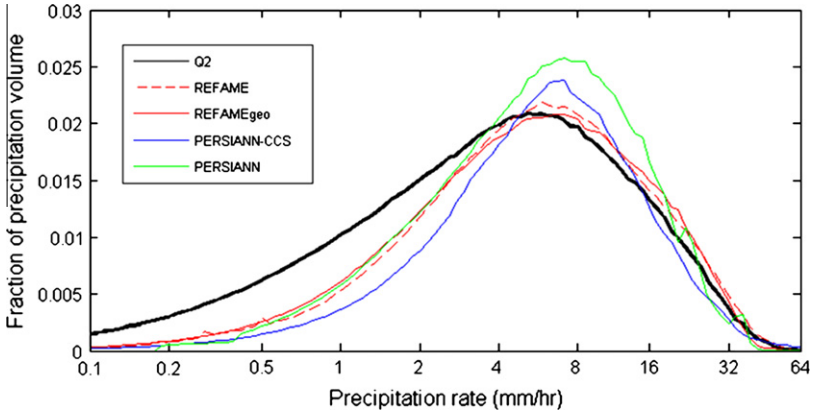

Fig. 2. Fractions of precipitation volume (*y*-axis) versus precipitation intensity (*x*-axis) derived from half-hour REFAME, REFAMEgeo, PERSIANN, and PERSIANN-CCS products. Only precipitation rates between 0.1 mm/hr and 64 mm/hr are included in Fig. 2, and the precipitation fractions are calculated for 100 evenly divided precipitation-intensity bins in logarithmic scale.

Table 1 provides more detailed quantitative and categorical statistics for REFAME, REFAMEgeo, PERSIANN, and PERSIANN-CCS for the summer months of 2009 and 2011 over the contiguous United States. A detailed description of the quantitative and categorical statistics calculated in Table 1 is provided in Appendix A. The quantitative statistics include correlation coefficient (COR), root-mean-square error (RMSE), and volume bias (BIASv). Categorical statistics, on the other hand, are calculated from the contingency table and through identifying binary (1/0 or yes/no) flags for rain/no-rain grid boxes and include equitable threat score (ETS), probability of detection (POD), false-alarm ratio (FAR), and areal bias (BIASa). The statistics are derived from corresponding maps of 30-min precipitation rates at 0.08-, 0.25-, 0.5-, and 1-degree latitude/longitude resolutions; Q2 precipitation data are used as ground reference. Note that, because the highest resolution offered by PERSIANN is 0.25°, statistical scores for PERSIANN are not included in the 0.08-degree resolution table. Comparison of REFAMEgeo with REFAME and PERSIANN-CCS suggests that the weighted-averaging of the GEO-based precipitation estimate with REFAME is effective and overall results in favorable categorical scores among the other products. At 0.25-degree resolution, REFAMEgeo demonstrates approximately 10%, 42%, and 31% gains in ETS over REFAME, PERSIANN-CCS, and PERSIANN, respectively. Note that, as opposed to individual categorical statistics, ETS allows the scores to be compared "equitably" across different regimes (Schaefer, 1990) and could be used as a good measure for overall performance of the products to delineate precipitation areas. The comparison is not necessarily representative if individual scores are compared. For example, while BIASa = 1 indicates that predicted and observed precipitation areas are identical, it does not necessarily indicate a perfect match between rain/no-rain grid boxes of observed and predicted fields. By cross-comparing the quantitative statics, it is also observed that REFAMEgeo outperforms other products, including REFAME. At 0.25-degree resolution, for example, REFAMEgeo demonstrates approximately 13%, 42%, and 24% gains in COR over REFAME, PERSIANN-CCS, and PERSIANN, respectively. In terms of RMSE, REFAMEgeo is also compared favorably with other products. Assessment of the BIASv across different spatial resolutions suggests that PERSIANN-CCS has the best BIASv, while PERSIANN shows more than 30% overestimation of precipitation volume. REFAMEgeo and REFAME show about 15% and 20% overestimations of precipitation volume across different resolutions, slightly higher than that obtained from PERSIANN-CCS.

Quantitative and categorical statistics for half-hour pairs of instantaneous combined MW (obtained from MWCOMB) and Q2 rain products are also shown in Table 2. While the combined MW rain estimate shows large volume Bias (BIASv), it displays an overall higher skill than any other high resolution products (compare Tables 1 and 2). For example, at 0.08° resolution, the combined MW product shows ETS and COR of about 0.34 and 0.45 which are about 10% and 13% higher than those obtained from REFAMEgeo. The lower skill of the high resolution products comes at the expense of covering about 67% of the areas (on average every half-hour for summer months of 2009 and 2011) over the contiguous United States that are not observed by the combined MW

Table 1
Quantitative and categorical statistics for REFAME, REFAMEgeo, PERSIANN, and PERSIANN-CCS for the 3 months (June, July, and August) of the summer of 2009 and 2011 over the contiguous United States. Statistics are calculated from half-hour pairs of satellite and Q2 products.

	ETS	POD	FAR	BIASa	COR	RMSE (mm/hr)	BIASv
0.08°							
REFAME	0.29	0.45	0.48	0.86	0.35	1.31	1.26
REFAMEgeo	0.31	0.50	0.48	0.95	0.40	1.20	1.12
PERSIANN-CCS	0.21	0.33	0.46	0.61	0.29	1.33	1.03
0.25°							
REFAME	0.31	0.50	0.48	0.96	0.45	1.05	1.24
REFAMEgeo	0.34	0.53	0.45	0.96	0.51	0.94	1.11
PERSIANN-CCS	0.24	0.36	0.49	0.70	0.36	1.03	1.02
PERSIANN	0.26	0.41	0.51	0.85	0.41	1.00	1.14
0.50°							
REFAME	0.34	0.53	0.43	0.93	0.54	0.87	1.24
REFAMEgeo	0.37	0.55	0.39	0.91	0.59	0.77	1.09
PERSIANN-CCS	0.27	0.42	0.46	0.77	0.45	0.83	1.00
PERSIANN	0.29	0.48	0.49	0.94	0.51	0.81	1.14
1°							
REFAME	0.39	0.58	0.36	0.90	0.63	0.68	1.23
REFAMEgeo	0.43	0.60	0.30	0.86	0.68	0.61	1.09
PERSIANN-CCS	0.32	0.50	0.41	0.86	0.56	0.62	0.99
PERSIANN	0.33	0.52	0.40	0.88	0.62	0.63	1.13

Table 2
Quantitative and categorical statistics calculated from half-hour pairs of MWCOMB and Q2 rain products for summer months (June, July, and August) of 2009 and 2011 over the contiguous United States.

	ETS	POD	FAR	BIASa	COR	RMSE (mm/hr)	BIASv
0.08°	0.34	0.47	0.39	0.78	0.45	1.31	1.41
0.25°	0.40	0.57	0.37	0.91	0.60	0.88	1.45
0.50°	0.44	0.61	0.33	0.92	0.67	0.74	1.44
1.00°	0.49	0.67	0.28	0.93	0.73	0.59	1.40

products. Arguably, the role of the combined high resolution products in providing a near real-time complete spatiotemporal coverage of rapidly-evolving hydrometeorological events is critical for hydrologic applications such as flash floods which primarily occur during summer/warm seasons. It is important to note that because the evaluation of MWCOMB and the merged products are performed at high spatiotemporal resolutions it is likely that errors in ground radar precipitation estimates as well as satellite ground misregistration issues (Villarini et al., 2009; Kidd et al., 2003) significantly reduce the reported skills.

As the time distance from previous MW overpasses increases, GEO-based precipitation gains more weight in the combination procedure employed in REFAMEgeo. Therefore, REFAMEgeo is less vulnerable to decline in number of accessible MW overpasses in near real-time operation. This issue is shown in Fig. 3a, where COR of 0.08°-resolution REFAMEgeo, REFAME, and PERSIANN-CCS with reference Q2 are compared with respect to the time distance from previous MW overpasses. Fig. 3b displays the number of samples used to calculate the correlation coefficients. Fig. 3a shows that, as the time distance from previous MW overpasses increases, the COR score drops considerably for REFAME. However, REFAMEgeo is much less vulnerable to the time distance from previous MW overpasses and consistently outperforms both REFAME and PERSIANN-CCS across all time distances. This is an important feature of REFAMEgeo that makes it suitable for near real-time operation. PERSIANN-CCS is independent of time distance from MW overpass because it only relies on Tb which is available every half-hour through GEO satellite. Note that approximately one hour after the previous MW overpass COR of REFAME becomes smaller than PERSIANN-CCS. This suggests that, farther in time from MW overpass, the combination of REFAME with GEO-based precipitation employed in REFAMEgeo is essential to maintain the performance of the retrieved precipitant above that can be obtained from GEO-only or MW-only estimates.

As a case study, the statistical scores for three representative days (August 5–7, 2009) are shown in Fig. 4. The statistics are derived at half-hour 0.25-degree resolution from corresponding maps of REFAMEgeo, PERSIANN, PERSIANN-CCS, and reference Q2 precipitation intensities. The left side panels show quantitative statistics, while the right side panels represent categorical statistics. Among the products, REFAMEgeo performs favorably, particularly with respect to COR, ETS, and POD, as shown in Fig. 4a, b, and d. Performance of REFAMEgeo with respect to RMSE (Fig. 4c), BIASa (Fig. 4g), and FAR (Fig. 4f) is also remarkable. Indicated by ETS (Fig. 4b) as an overall detection score, it can be concluded that REFAMEgeo outperforms PERSIANN and PERSIANN-CCS to capture both precipitations' areal extent and location. REFAMEgeo shows considerably higher POD (Fig. 4d) and comparable FAR (Fig. 4f) compared to PERSIANN and PERSIANN-CCS. Fig. 4e shows that PERSIANN-CCS has the best BIASv, while PERSIANN shows a relatively significant overestimation of precipitation volume. Note that both PERSIANN and PERSIANN-CCS almost consistently underestimate the areal extent of precipitation (BIASa), while REFAMEgeo is subject to moderate underestimation and overestimation of precipitation areas.

In Fig. 5, diurnal cycle of average precipitation intensities during the summers of 2009 and 2011 over the contiguous United States is shown. The *x*-axis shows half-hour local time bins. Within each bin, 1-degree resolution precipitation intensities (including zero) are averaged and the resulted average-intensities are shown in *y*-axis. As evident from Fig. 5, the overall pattern is captured by all of the products. However, significant overestimation of average precipitation intensities is observed from late afternoon to early morning. The observed over estimation is more significant for PERSIANN compared to the other products across all hours except around noon, when PERSIANN shows minor underestimation of rain rates. In comparison to PERSIANN, PERSIANN-CCS and to a lesser extent REFAMEgeo show substantial underestimation of average rain rates from early morning to early afternoon. Q2 suggests that the minimum and maximum precipitation intensities take place around 10:30 am and 4:00 pm, respectively. While most of the products capture the time of the minimum precipitation

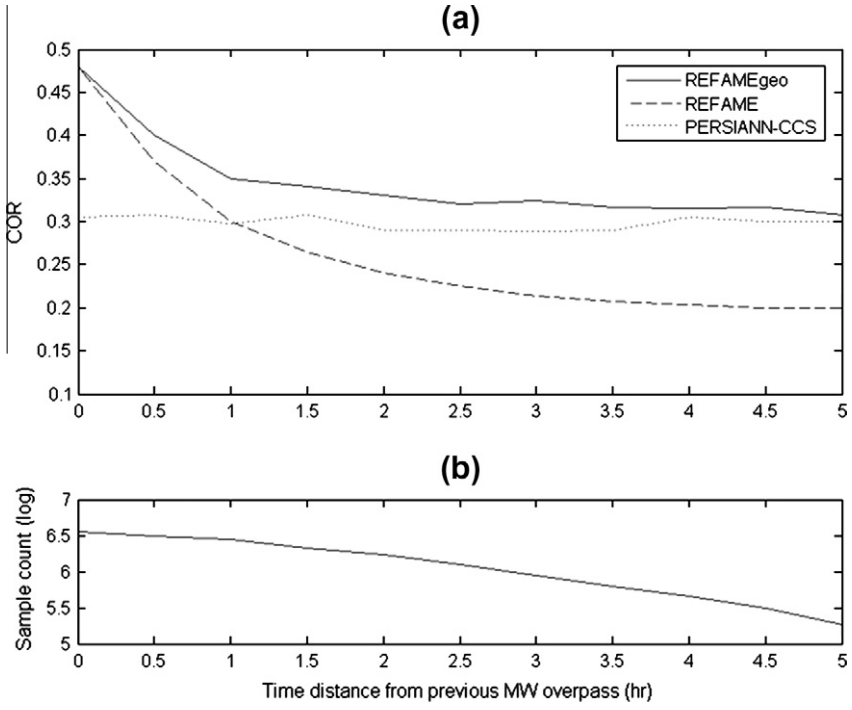

Fig. 3. (a) Comparison among the correlation coefficient of REFAMEgeo, REFAME, and PERSIANN-CCS with respect to time-distance from the most recent MW overpass, (b) number of samples at each time-distance used to derive the correlation coefficients reported in panel (a). The figure is constructed using half-hour 0.08° latitude/longitude precipitation data from 2009.

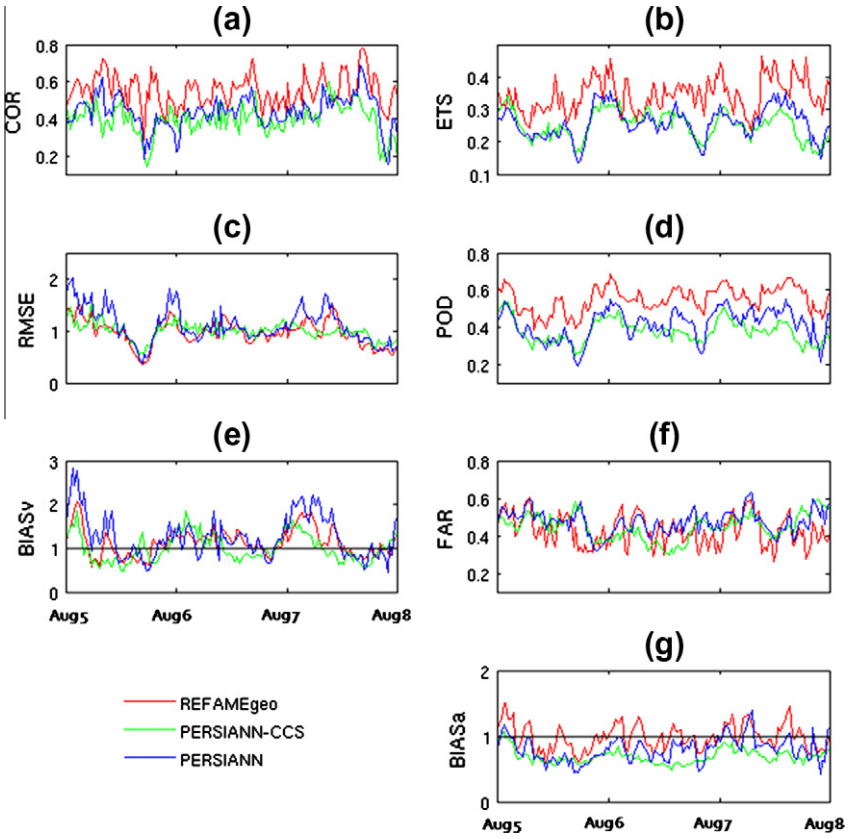

Fig. 4. Statistical measures for REFAMEgeo, PERSIANN-CCS, and PERSIANN during August 5–7, 2009. The statistics are derived at half-hour 0.25-degree resolution from corresponding maps of the satellite products and reference Q2 precipitation intensities. The left-side panels show quantitative statistics: (a) COR, (c) RMSE, and (e) BIASv, while the right-side panels display categorical statistics: (b) ETS, (d) POD, (f) FAR, and (g) BIASa.

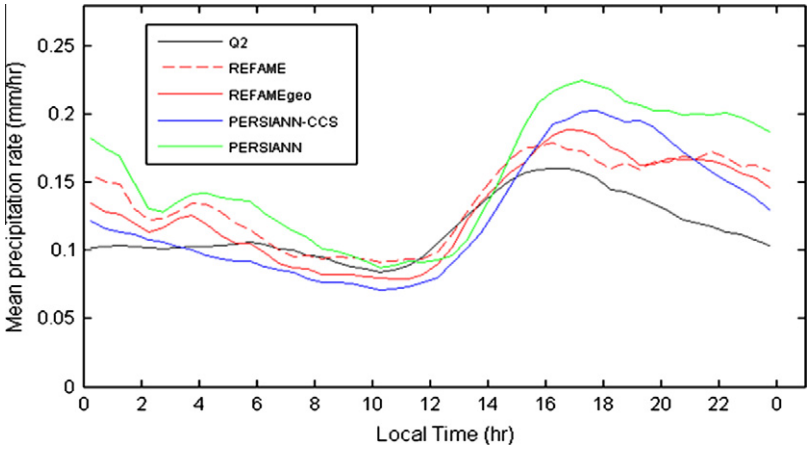

Fig. 5. Diurnal cycle of average precipitation intensities during the summer months of 2009 and 2011 over the contiguous United States. The *x*-axis shows the half-hour local time bins. Within each bin, 1-degree resolution precipitation intensities (including zero) are averaged and the resulted average-intensities are shown in *y*-axis.

intensity, they demonstrate a broad peak approximately between 4:00 pm. and 5:30 pm. local time. REFAME agrees well with Q2 between 6:00 am. and 2:00 pm. local time and together with the other products overestimates precipitation intensities during late afternoon and early morning. From Fig. 5, it is observed that, within the rising limb of the diurnal cycle curve, the products agree well among themselves. However, they start to exhibit large discrepancies a few hours later, when a majority of convective precipitation systems start to grow. Note that unlike PERSIANN-CCS, REFAME, REFAMEgeo and PERSIANN show local minimums around 2 am where Q2 diurnal cycle is almost flat. The reason for this is under investigation and might be relevant to the MW inputs that are not used in PERSIANN-CCS.

5. Summary and concluding remarks

In the present study, two recently developed algorithms for near real-time high-resolution precipitation estimation (REFAME and its variation REFAMEgeo) are evaluated during the summers of 2009 and 2011 over the contiguous United States. Within a Lagrangian framework, REFAME generates precipitation rates by adjusted advection of MW-derived precipitation intensities using

radiative and textural features extracted from more frequent GEO-IR images. A variant of REFAME, REFAMEgeo provides precipitation intensities through weighted averaging of REFAME and precipitation estimates derived from GEO-IR. The latter approach also allows including precipitation events that may be missed in previous MW overpasses. The weights are identified by considering the performance of each combination component and the time distance from previous MW overpasses. Both REFAME and REFAMEgeo generate precipitation intensities at 0.08-degree latitude/longitude resolution, every half-hour. In the present study, two half-hour real-time high-resolution precipitation products (PERSIANN and PERSIANN-CCS) were considered for comparison with REFAME and REFAMEgeo. The Q2 precipitation data, developed at the NOAA/National Severe Storms Laboratory in cooperation with the University of Oklahoma, were used as reference ground truth. The evaluations were performed at half-hour temporal resolution and at a range of spatial resolutions (0.08-, 0.25-, 0.5-, and 1-degree latitude/longitude). Overall, for the period and location of the study, REFAMEgeo performs well among the studied products to estimate precipitation intensity as well as to detect occurrence of precipitation events. Cross-comparison among REFAME, REFAMEgeo, and PERSIANN-CCS suggests that REFAMEgeo has a robust performance, particularly as the time distance from previous MW overpasses increases. Compared to REFAME it is found that REFAMEgeo maintains its skill relatively well as the time distance from previous MW overpasses increases. This is an important feature of REFAMEgeo that makes it suitable for near real-time operations where a large decline in the number of accessible MW overpasses is probable. Despite REFAMEgeo's robust performance, it does not replace the critical need for a sufficient number of MW sensors with proper equator-crossing times to overcome adverse impacts of time distance between MW overpasses. To a large extent, this demand will be addressed after the successful launch and operation of the Global Precipitation Measurement (GPM) mission (Hou et al., 2008).

With respect to precipitation quantity, REFAMEgeo and REFAME demonstrate slight overestimation of intense precipitation and underestimation of light precipitation events. Inclusion of a near-real-time bias-reduction (e.g., Tian et al., 2010) procedure is under investigation since bias-adjusted products can lead to substantial improvement in many applications such as hydrologic simulation of streamflow (e.g., Behrangi et al., 2011 among others). In the present study, REFAME and REFAMEgeo only relied on IR ($\sim$11 μm) data to adjust the intensity of MW precipitation estimates as advected forward. However, previous studies (Ba and Gruber, 2001; Behrangi et al., 2009, among others) have shown that additional GEO VIS/IR and water–vapor channels can advance classification of clouds and, as a result, may lead to further improvement in the delineation of areal extent and estimation of precipitation intensity. With the emergence of modern imagers on recent and future geostationary satellites (e.g., SEVERI on MSG and the Advanced Baseline Imager (ABI) on GOES-R), more spectral channels with higher spatial and temporal resolution are becoming available. Future research directed to comprehensive assessment of the role of multi-spectral information in improving algorithms, such as REFAME and REFAMEgeo, is ongoing. In addition, development, refinement, and testing of REFAME and REFAMEgeo for global operation are currently underway at the Center for Hydrometeorology and Remote Sensing (CHRS) at the University of 'California, Irvine.

Acknowledgments

Partial financial support was provided by the NASA-PMM (Grant NNX10AK07G), and the NASA NEWS (Grant NNX06AF934), and the US Army Research Office project (Grant W911NF-11-1-0422). The authors thank Dan Braithwaite and Eyal Amitai for their technical assistance on processing the satellite/radar data for this experiment. Part of the research was carried out at the Jet Propulsion Laboratory, California Institute of Technology, under a contract with the National Aeronautics and Space Administration.

Appendix A. Definition of the statistical measures used in this study

A.1. Quantitative statistics

If PR_{est} and PR_{obs} represent estimated and observed precipitation rates, the quantitative statistics used in the present work are defined below:

$$\text{Correlation coefficient (COR)} = \frac{\sum_{i=1}^{N}((PR_{obs})_i(PR_{est})_i) - [N(\overline{PR}_{obs})(\overline{PR}_{est})]}{\sqrt{\left[\sum_{i=1}^{N}(PR_{obs})_i^2 - N(\overline{PR}_{obs})^2\right]\left[\sum_{i=1}^{N}(PR_{est})_i^2 - N(\overline{PR}_{est})^2\right]}}$$

$$\text{Root-mean-square-error (RMSE)} = \left(\frac{1}{N}\sum_{i=1}^{N}(PR_{est}(i) - PR_{obs}(i))^2\right)^{0.5}$$

$$\text{Volume bias (BIASv)} = \frac{\sum_{i=1}^{N}(PR_{est}(i) - PR_{obs}(i))}{N}$$

where N is the total number of observed and estimated precipitation pairs.

A.2. Categorical statistics

Categorical statistics are calculated from the binary-based contingency table. The table classifies the prediction results into the following four possibilities based on observation of precipitation or no-precipitation occurrences:

(1) Hit (H): number of pixels correctly classified as precipitation.
(2) Miss (M): number of pixels incorrectly classified as no precipitation.
(3) False alarm (F): number of pixels incorrectly classified as precipitation.
(4) Correct negative (Z): number of pixels correctly classified as no precipitation.

A perfect prediction system would produce only hits and correct negatives and no misses or false alarms. However, in reality, predictions are not perfect. The prediction skill can be evaluated based on indices derived from the contingency table. Among the most commonly used statistics are:

$$\text{Probability of detection (POD)} = H/(H+M)$$

$$\text{False alarm ratio (FAR)} = F/(H+F)$$

$$\text{Areal bias (BIASa)} = (H+F)/(H+M)$$

where H = hits, F = false alarm, M = misses, and Z = correct negative, as defined above. POD and FAR range from 0 to 1, with perfection represented by a POD of one, together with a FAR of 0. POD is sensitive to the number of hits, but it ignores false alarms; FAR, on the

other hand, is sensitive to false alarms, but it ignores misses. BIASa considers both predictions and observations. A value of one indicates that predictions and observations have identical areal coverage independent of location. However, a perfect BIASa score does not necessarily indicate a perfect skill of the predictor for correct delineation of rain areas from no-rain areas.

References

Ba, M.B., Gruber, A., 2001. GOES multispectral rainfall algorithm (GMSRA). J. Appl. Meteorol. 40 (8), 1500–1514.

Behrangi, A., Hsu, K., Imam, B., Sorooshian, S., Huffman, G.J., Kuligowski, R.J., 2009. PERSIANN-MSA: a precipitation estimation method from satellite-based multispectral analysis. J. Hydrometeorol. 10, 1414–1429.

Behrangi, A., Imam, B., Hsu, K., Sorooshian, S., Bellerby, T., Huffman, G.J., 2010. REFAME: rain estimation using forward adjusted-advection of microwave estimates. J. Hydrometeorol. 11 (6), 1305–1321.

Behrangi, A., Khakbaz, B., Jaw, T.C., AghaKouchak, A., Hsu, K., 2011. Sorooshian, S., Hydrologic evaluation of satellite precipitation products over a mid-size basin. J. Hydrol. 397 (3–4), 225–237.

Bellerby, T.J., 2006. High-resolution 2-D cloud-top advection from geostationary satellite imagery. IEEE Trans. Geosci. Remote Sensing 44 (12), 3639–3648.

Bellerby, T., Hsu, K., Sorooshian, S., 2009. LMODEL: a satellite precipitation methodology using cloud development modeling. Part I: algorithm construction and calibration. J. Hydrometeorol. 10 (5), 1081–1095.

Ferraro, R.R., 1997. Special sensor microwave imager derived global rainfall estimates for climatological applications. J. Geophys. Res. 102 (D14), 16715–16735.

Hong, Y., Hsu, K., Sorooshian, S., Gao, X.G., 2004. Precipitation estimation from remotely sensed imagery using artificial neural network cloud classification system. J. Appl. Meteorol. 43 (12), 1834–1853.

Hou, A.Y., Skofronick-Jackson, G., Kummerow, C., Shepherd, M., 2008. Global precipitation measurement. In: Michaelides, Silas (Ed.), Precipitation: Advances in Measurement, Estimation and Prediction. Springer Verlag, ISBN 978-3-540-77654-3, pp. 131–164 (Chapter).

Hsu, K.L., Gao, X.G., Sorooshian, S., Gupta, H.V., 1997. Precipitation estimation from remotely sensed information using artificial neural networks. J. Appl. Meteorol. 36 (9), 1176–1190.

Huffman, G.J., Adler, R.F., Bolvin, D.T., Gu, G.J., Nelkin, E.J., Bowman, K.P., Hong, Y., Stocker, E.F., Wolff, D.B., 2007. The TRMM multisatellite precipitation analysis (TMPA): quasi-global, multiyear, combined-sensor precipitation estimates at fine scales. J. Hydrometeorol. 8, 38–55.

Joyce, R.J., Janowiak, J.E., Arkin, P.A., Xie, P., 2004. CMORPH: a method that produces global precipitation estimates from passive microwave and infrared data at high spatial and temporal resolution. J. Hydrometeorol. 5 (3), 487–503.

Kidd, C., Kniveton, D.R., Todd, M.C., Bellerby, T.J., 2003. Satellite rainfall estimation using combined passive microwave and infrared algorithms. J. Hydrometeorol. 4 (6), 1088–1104.

Kuligowski, R.J., 2002. A self-calibrating real-time GOES rainfall algorithm for short-term rainfall estimates. J. Hydrometeorol. 3 (2), 112–130.

Nikolopoulos, E.I., Anagnostou, E.N., Hossain, F., Gebremichael, M., Borga, M., 2010. Understanding the scale relationships of uncertainty propagation of satellite rainfall through a distributed hydrologic model. J. Hydrometeorol. 11 (2), 520–532.

Schaefer, J.T., 1990. The critical success index as an indicator of warning Skill. Weather Forecast. 5 (4), 570–575.

Sorooshian, S. et al., 2000. Evaluation of PERSIANN system satellite-based estimates of tropical rainfall. Bull. Am. Meteorol. Soc. 81 (9), 2035–2046.

Tian, Y., Peters-Lidard, C.D., Eylander, J.B., 2010. Real-time bias reduction for satellite-based precipitation estimates. J. Hydrometeorol. 11 (6), 1275–1285.

Turk, F.J. et al., 2000, Combining SSM/I, TRMM and infrared geostationary satellite data in a near real-time fashion for rapid precipitation updates: advantages and limitations. In: Proc., EUMETSAT Meteorological Satellite Data Users' Conf., vol. 2, Bologna, Italy, EUMETSAT, pp. 705–707.

Ushio, T. et al., 2009. A Kalman filter approach to the global satellite mapping of precipitation (GSMaP) from combined passive microwave and infrared radiometric data. J. Meteorol. Soc. Jpn. 87A, 137–151.

Vasiloff, S.V. et al., 2007. Improving QPE and very short term QPF: an initiative for a community-wide integrated approach. Bull. Am. Meteorol. Soc. 88 (12), 1899–1911.

Vila, D., Ferraro, R., Joyce, R., 2007. Evaluation and improvement of AMSU precipitation retrievals. J. Geophys. Res.-Atmos. 112 (D20), 14.

Villarini, G., Krajewski, W.F., Smith, J.A., 2009. New paradigm for statistical validation of satellite precipitation estimates: application to a large sample of the TMPA 0.25 3-hourly estimates over Oklahoma. J. Geophys. Res. 114, D12106. http://dx.doi.org/10.1029/2008JD011475.

Wilheit, T., Kummerow, C.D., Ferraro, R., 2003. NASDARainfall algorithms for AMSR-E. IEEE Trans. Geosci. Remote Sens. 41 (2), 204–214.

World Water Assessment Programme, 2009. The United Nations World Water Development Report 3: Water in a Changing World. Paris:UNESCO, and London, Earthscan.

Zhang, J., Howard, K., Vasiloff, S., et al., 2009. National Mosaic and multi-sensor QPE (NMQ) system: description, results and future plans. In: The 34th Conf. on Radar Meteorology. Amer. Meteor. Soc. 5–9 October 2009, Williamsburg, VA. Paper 7A.1.